Photovoltaic Effect in Indium(I) Iodide Thin Films

Wiley A. Dunlap-Shohl,[†] Ian G. Hill,[‡] Yanfa Yan,[⊥] David B. Mitzi*,[†,§]

† Department of Mechanical Engineering and Materials Science, Duke University, Durham, North Carolina 27708, United States

‡ Department of Physics and Atmospheric Sciences, Dalhousie University, Halifax, Nova Scotia B3H 3J5, Canada

⊥ Department of Physics and Astronomy and Center for Photovoltaics Innovation and Commercialization, The University of Toledo, Toledo, Ohio 43606, United States

§ Department of Chemistry, Duke University, Durham, North Carolina 27708, United States

ABSTRACT: Halide semiconductors are undergoing a period of intense interest, buoyed by the outstanding optoelectronic properties of hybrid perovskites. It is worthwhile to consider whether related materials sharing unique aspects of the perovskite chemistry, such as the incorporation of metals that provide lone pair s electrons when integrated within the halide lattice, might yield semiconductors with comparable properties. One such metal that has not been widely studied in the context of photovoltaics is monovalent indium. In this work, we investigate a method of depositing films of indium(I) iodide, coupled with optoelectronic characterization and incorporation of these films into thin-film solar cells. We find that, although indium(I) iodide exhibits a photovoltaic effect, it is likely to be compromised by difficult-to-remove defects, e.g., iodine vacancies, which are expected to introduce recombination centers deep within the band gap.

The extraordinary optoelectronic and photovoltaic properties of the halide perovskite family have stimulated an interest in uncovering their physical origins and investigation of new materials with similar chemistry and, ideally, similar properties. One attribute that has been suggested to underpin the high optoelectronic quality of these materials is the contribution of lone pair electrons from the metal to the valence band (*e.g.*, $6s^2$ electrons from Pb). This feature is proposed not only to make the valence band more dispersive, leading to a low hole effective mass, but also to improve defect tolerance due to the antibonding coupling between the metal lone pair s and halide p orbitals.[1] It is thus reasonable to inquire which lone pair-containing metals beyond Pb/Sn may be integrated into similar crystal structures, and whether such materials might possess the outstanding semiconducting properties of the halide perovskites. Such metals include In^+ and Sb^{3+}, or Tl^+ and Bi^{3+}, which are isoelectronic to Sn^{2+} and Pb^{2+}, respectively. Sb^{3+} and Bi^{3+} have enjoyed some limited photovoltaic success when integrated into reduced-dimensional perovskites ($A_3Bi_2I_9$ or $A_3Sb_2I_9$, where A is methylammonium or an alkali metal such as Rb),[2-5] the double perovskite $Cs_2AgBiBr_6$,[6] or related halide semiconductors such as BiI_3[7], BiOI,[8] or $Ag_aBi_bI_{a+3b}$.[9-11] While the addition of small amounts of Tl appears to reduce the band gap of $Cs_2AgBiBr_6$ to values more suitable for photovoltaics,[12] it is highly toxic and therefore an undesirable replacement for Pb. However, despite some discussion in the context of radiation detectors,[13-14] and a recent report by Brandt *et al.*[15] suggesting that the carrier lifetime of InI compares favorably with other Pb-free halide semiconductors of interest for solar cells, the photovoltaic properties of In^+-containing materials are underexplored, and the lower toxicity of In makes it an interesting candidate for investigation (with the caveat that In is a relatively scarce element, with abundance in the Earth's crust about equal to that of Ag, and market price >$200/kg in 2017).[16-17]

In this work, we focus on InI, one of the simplest In^+-containing halide semiconductors. InI has a crystal structure that is similar to the rock salt structure, but it is staggered every two atomic sheets such that the In atoms in one layer are more closely bonded to the In atoms in the adjacent layer, as opposed to the I atoms, as shown in Figure 1a.[18] Thus, each I atom is coordinated to five In atoms in distorted square pyramidal geometry, while each In atom is coordinated to five I atoms, also in distorted square pyramidal geometry, and additionally to two In atoms in the adjacent layer. The relatively strong bonding between the two-layer "slabs" results in a more 3-dimensional structure than would be typically expected for such a layered compound.[18] As the lone pair metal and the halogen are the

dominant contributors to the valence and conduction band edges in halide perovskites,[1, 19-20] it is reasonable to inquire whether InI might lead to a replication of favorable band structure properties.

While the band gap of InI is reported as ~2.0 eV,[18] slightly wider than ideal for single-junction photovoltaics, this material could in principle prove useful as the top cell in a tandem architecture, or otherwise in light-emitting applications. Prior calculations indicate that InI has a direct band gap with dispersive band edges.[15, 21-22] This feature arises as a result of hybridization between the In 5*s* and I 5*p* orbitals in the valence band, and the cationic character of the In 5*p* orbitals in the conduction band.[22-23] However, defect calculations by Biswas and Du[18] have indicated that the presence of Schottky defects (*i.e.*, paired vacancies of In and I, V_{In} and V_I) may be troublesome, due to pinning of the Fermi level near mid-gap and the probable behavior of V_I as a deep electron trap. Shi and Du[24] indicate that, despite the presence of n*s*^{2} cations, InI lacks an appropriate structure to protect against formation of deep V_I, as the neighboring In 5*p* orbitals all point toward the center of the vacancy and may thus easily hybridize to form a localized state. More recent calculations indicate that V_I has a low formation enthalpy,[15, 25] and Kurchin *et al.*[25] propose that the presence of a lone pair metal in binary metal halides can lead to shallow cation vacancies but does not preclude deep anion vacancies. However, experimental reports of reasonably high carrier lifetimes[15] (~6 ns) and mobility-lifetime products[13, 26] ($\mu\tau$ on the order of 10^{-4} cm^2/V) in InI single crystals suggest that this material may nonetheless be suitable for photovoltaic energy conversion in thin-film devices. Assuming an Einstein relation between carrier mobility μ and diffusion coefficient ($D = \mu k_B T/q$), the above $\mu\tau$ should correspond to a carrier diffusion length $L_D = \sqrt{D\tau}$ of ~16 μm. As the absorber in thin-film solar cells is generally no more than 1–2 μm thick, such a diffusion length should be more than adequate for efficient carrier collection. It is therefore worthwhile to investigate whether InI might serve as a promising optoelectronic material, and to develop ways of depositing and characterizing thin films of this material. In this work, we discuss the properties of InI thin films prepared by thermal evaporation, and assess the performance of solar cells based on these films.

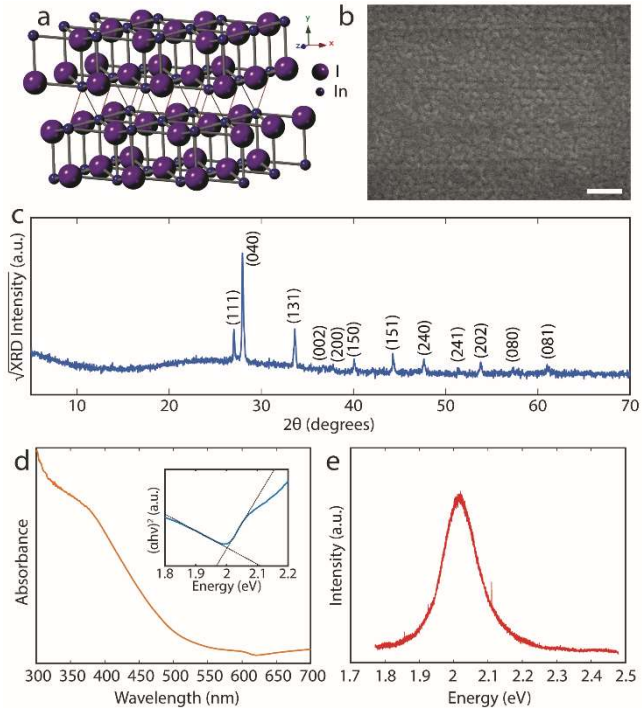

Figure 1. Crystal structure (a) of InI, drawn using CrystalMaker® software. Thick lines denote intra-slab In—I bonds, while thin lines denote inter-slab In—In bonds; SEM image (b) of an InI film on glass (scale bar: 500 nm); XRD pattern (c) of an InI film evaporated onto glass (plotted using a square root scale for ease of visualizing weak peaks), with all reflections indexed according to pattern 01-079-0534 in the International Centre for Diffraction Data database; UV-vis absorption spectrum (d) and Tauc plot (inset) of an InI film on glass, showing a direct band gap of 2.0 eV; PL spectrum (e) of an InI film evaporated onto glass and encapsulated with an overlying poly(methyl methacrylate) (PMMA) film, exhibiting band-to-band luminescence.

Because InI is sparingly soluble in common organic solvents and also is liable to oxidize easily due to the relative instability of In^+ relative to In^{3+}, we have chosen to use a physical (*i.e.*, single-source thermal evaporation) rather than chemical method to deposit InI. The as-deposited films (on soda-lime glass substrates) were then characterized by X-ray diffraction (XRD), scanning electron microscopy (SEM), and UV-vis absorption and photoluminescence (PL) spectroscopies. Top-view SEM (Figure 1b) reveals a network of compact but very small grains, on the order of 100 nm. The XRD pattern (Figure 1c) of the as-deposited InI film is not dominated by reflections characteristic of any particular set of Miller indices, although the strongest peak belongs to the (040) reflection. This orientation corresponds to a configuration in which the layers of the InI crystal structure are parallel to the glass substrate. Such a configuration may be expected to dominate intuitively, as it is typical for layered compounds to favor alignment of the basal planes with the substrate; in fact, from this perspective, the extent to which other reflections are evident is somewhat surprising. However, the strength of inter-layer bonding in InI (as reflected by the

slab-to-slab In—In bonds being only slightly longer than the In—I bonds) contributes to a reduced anisotropy of this material relative to other layered compounds of similar chemistry (*e.g.*, PbI_2 or BiI_3).[18, 22]

The UV-vis spectrum (Figure 1d) of the as-deposited film indicates an absorption onset at ~620 nm, while the corresponding Tauc plot (Figure 1d inset), assuming a direct transition, yields a band gap of 2.00 eV, in good agreement with previous reports.[13, 18] At wavelengths below that corresponding to the band gap, the absorption increases monotonically in a manner resembling that of other semiconducting halides such as $CH_3NH_3PbI_3$. Note that there also appears to be an increase in absorption for wavelengths above the band gap. Plotting the UV-vis-NIR spectra of InI films of different thicknesses reveals that this effect is most likely due to thin film interference, as evidenced by the shifting maxima and minima in the infrared regime (Figure S1). These effects are also discernible in the visible/below band gap range, but absorption is clearly the dominant effect here, as evidenced by roughly linear scaling of the absorbance with film thickness. The PL spectrum (Figure 1e) of the InI film peaks relatively close to the band gap value, at 2.02 eV, and is thus likely characteristic of band-to-band recombination; however, the PL response is relatively weak, possibly indicating a large density of recombination centers. We also note that, although it is generally possible to obtain reasonable PL spectra from InI films, they are easily damaged by the 442 nm laser used to excite them, and care must therefore be taken when collecting and comparing these spectra. In general, these films are highly unstable in air, showing visible signs of decomposition within 3 h of continuous exposure to ambient atmosphere (relative humidity ~50% at room temperature).

Ultraviolet and inverse photoemission spectroscopy (UPS and IPES) of an InI film evaporated onto indium tin oxide (ITO) were used to characterize band positions and work function, as shown in Figure 2. From the secondary electron cutoff at 16.4 eV below the Fermi level (Figure 2a) in the He I ($h\nu$ = 21.2 eV) UPS spectrum, the work function is estimated to be 4.8 eV. Fitting the valence band edge in the UPS spectrum yields an ionization energy of 5.6 eV, placing the Fermi level nearly at midgap, while the IPES spectrum suggests an electron affinity of ~3.6 eV (obtained by fitting the signal as a sum of gaussians representing the conduction band density of states with an exponential function representing the background). The fundamental band gap, established by the 2.0 eV difference between the ionization energy and the electron affinity, agrees with the optical band gap measured by UV-vis, within the limits of experimental error. These measurements also agree closely with the defect calculations of Biswas and Du,[18] which suggest that native Schottky defects should pin the Fermi level ~0.8 eV above the valence band. This result is thus consistent with these defects being active within the evaporated InI films; V_I defects may possibly account for the observed weak PL.

X-ray photoelectron spectroscopy (XPS) of the films deposited on both indium tin oxide (ITO) as well as glass substrates (the latter spectrum is shown in Figure 2c) demonstrates that, in addition to the expected contributions from indium, iodine, and adventitious carbon, a significant peak belonging to the oxygen 1*s* orbital appears, which may indicate the formation of a surface oxide. As noted above, the In^+ state is not as stable as In^{3+}, and it is possible that exposure to air when the film is loaded into the XPS tool may contribute to the presence of oxygen. However, oxygen is evident even in films that are deposited and transferred to the XPS chamber without air exposure, which suggests that it may originate from interactions of the film with trace moisture or O_2 in the evaporation chamber or gloveboxes. The I:In elemental ratio of 0.8 in the film grown on glass may simply reflect the competition amongst I^- and O^{2-} anions for coordination to In at the surface of the film. However, it is potentially concerning in view of the deep electron trap nature of V_I,[18] which may be present in large quantity in I-deficient films, providing an alternative possible explanation for the weakness of the PL emission. The presence of band-to-band PL, though weak, is nevertheless evidence of the photovoltaic potential of this material. It is therefore of interest to develop strategies that can improve the morphology and the optoelectronic properties of the InI films.

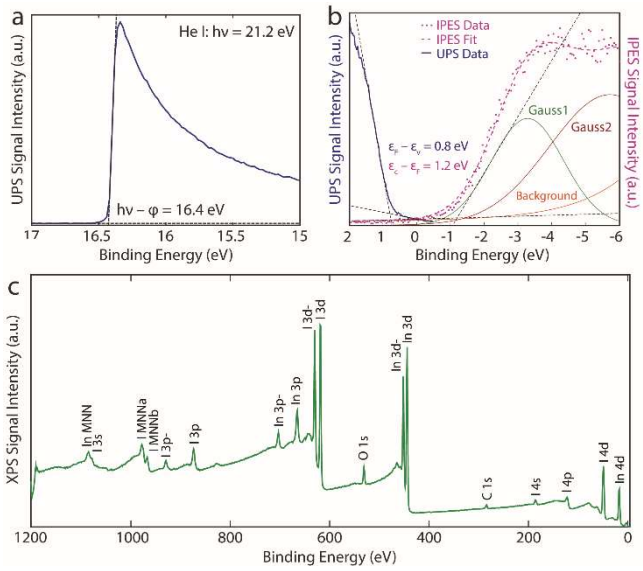

Figure 2. Photoelectron spectroscopy of InI films. Secondary electron cutoff region of the UPS spectrum (a) of an InI film evaporated onto ITO; band edge regions of an InI film on ITO (b) as measured by UPS (data: blue line) and IPES (data: purple dots, gaussian + exponential background fit: dashed purple line). Binding energies are referenced to the Fermi level. XPS spectrum (c) of an InI film on ITO, displaying contributions from In and I, as well as C and O.

One means of influencing the properties of vapor-grown films is to modify the substrate, which can have a substantial impact on the morphology and properties of the resulting films.[27] Strong crystallographic orientation of the substrate can be used to stimulate a similar degree of orientation in the overlying film (*e.g.*, epitaxy),[28] which may lead to improvement in the quality or functionality of that

film. The substrate need not possess a similar chemistry or crystal structure to the desired film in order to promote epitaxial growth, and may even be a thin film itself.[29-31] Alternatively, mobile species can diffuse from the substrate into the overlying film and affect its growth and material properties. Examples of such interactions have been observed in the perovskite literature for species such as Na[32] or Cd.[33-34] To modify the growth of InI, we employ a thin layer of SnI_2, which deposits with a heavily preferred orientation, as evidenced by the strong, evenly spaced series of reflections seen in Figure S2, and is chemically similar to InI (In^+ and Sn^{2+} are isoelectronic), which may reduce the chance of harmful defects arising from incorporation of Sn into the InI structure. SnI_2 is deposited onto the substrates by spin-coating from an N,N-dimethylformamide (DMF) solution in a nitrogen-filled glovebox, and thereafter annealing at 100 °C for 10 min to remove the solvent. We also compare the influence of amorphous soda-lime glass substrates relative to the half-solar cell stack of ITO/CdS, the latter of which is deposited using chemical bath deposition by a previously reported method.[33] CdS deposited in this manner is crystalline but with very small grains, as evidenced by previous work in which the only identifying feature in the X-ray diffraction pattern is a very weak and broad peak.[33]

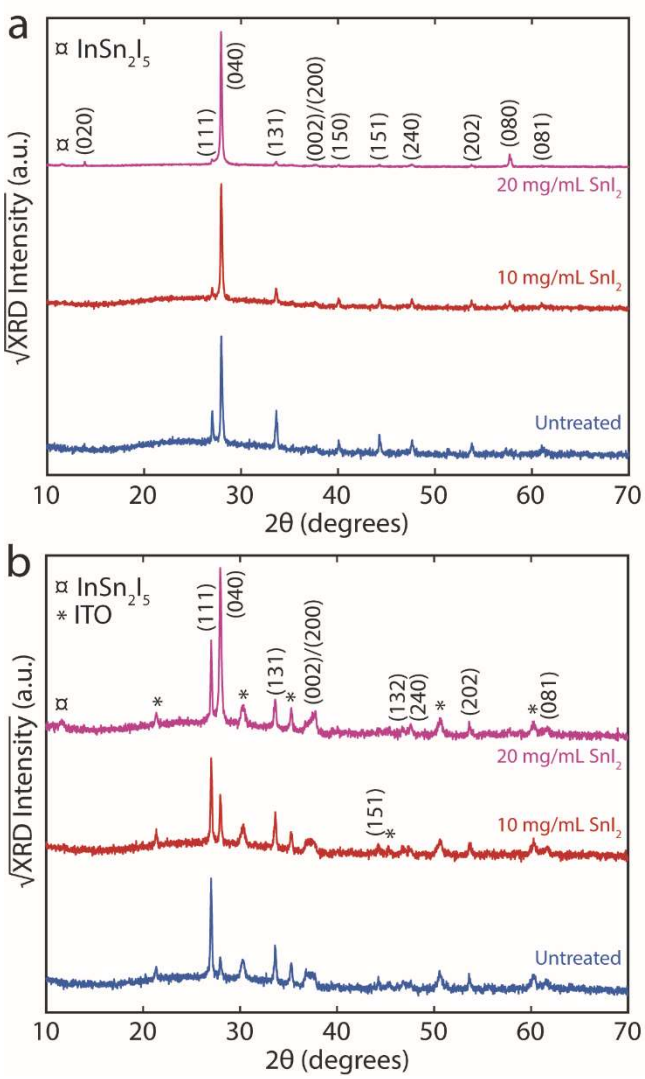

Figure 3. XRD patterns of InI films on various substrates with different SnI_2 treatments: soda-lime glass (a), and ITO/CdS (b). All patterns are plotted on square root scale to emphasize weaker peaks; patterns in (a) are normalized for ease of visualizing off-axis peaks.

When InI films are deposited onto a glass substrate treated with a 10 mg/mL SnI_2 solution, the (0*k*0) peaks in the XRD pattern of the InI film are strongly enhanced, while all other orientations are suppressed (Figure 3a). Increasing the SnI_2 concentration to 20 mg/mL further strengthens the (0*k*0) peaks relative to all other orientations, although the emergence of a weak peak at 2θ = 11.6° corresponds to the (002) peak of $InSn_2I_5$,[35-36] demonstrating spontaneous reaction between SnI_2 and InI. No such peak is evident in the pattern corresponding to the 10 mg/mL SnI_2 substrate. However, this observation does not preclude the possibility of such reaction happening in this case as well—i.e., the amount of $InSn_2I_5$ generated is most likely below the threshold of observation. When ITO/CdS substrates are used in place of glass, the preference for the (0*k*0) orientation is lessened relative to the others, and the (111) reflection dominates the InI component of the XRD pattern (Figure 3b). Nevertheless,

the SnI_2 treatment has the same effect on the InI film texture, with higher concentrations leading to an increasingly dominant (040) peak. The preferred orientation may, for example, be stimulated by epitaxial growth on the highly-oriented SnI_2 surface, or by the influence of diffused Sn on nucleation/growth of grains within the InI film. There do not appear to be any significant morphological differences in films fabricated on ITO/CdS substrates with different SnI_2 treatments, as seen in the SEM images in Figure S3.

Table 1. Elemental Ratios from Quantification of XPS Spectra of InI Films on ITO/CdS and Glass Substrates for Various Concentrations of SnI_2 Treatment (in mg/mL).

	glass			ITO/CdS		
SnI_2	**none**	**10**	**20**	**none**	**10**	**20**
I:In	**0.80**	**0.96**	**0.98**	**0.91**	**0.92**	**0.97**
I:O	**0.71**	**0.92**	**1.13**	**1.72**	**1.71**	**2.46**
Sn:In	**0.00**	**0.02**	**0.02**	**0.00**	**0.02**	**0.02**
Cd:In	**-**	**-**	**-**	**0.04**	**0.02**	**0.02**

A further interesting effect of the SnI_2 treatment is observed in the XPS spectra of the InI films (Figure S5). As noted above, the spectrum corresponding to the film on untreated glass contains a significant contribution from the O 1s peak, and an apparently I-deficient composition. Quantification of the elemental composition derived from these spectra is displayed in Table S1, and selected ratios of atomic percentages corresponding to different elements are given in Table 1. In films grown on the SnI_2-treated glass substrates, the I:In and I:O ratios tend to increase with SnI_2 concentration. Similar behavior is evident for the InI films on ITO/CdS substrates; while the difference between the untreated and 10 mg/mL SnI_2-treated substrates is marginal, the overall trend is clearly in the same direction as for the glass substrates. The correlation between the XRD and XPS results as a function of SnI_2 treatment is intriguing, and suggest a possible relationship between the (0*k*0) preferred orientation of the InI film and its elemental composition. For a surface of an InI crystallite corresponding to any orientation other than (0*k*0), dangling bonds will exist where oxygen can bond to indium atoms and displace iodine, or more easily oxidize and extract indium from the lattice during or after film deposition, since any plane not parallel to the rock salt slab structure must intersect some In—I bonds. Also, the van der Waals gaps between adjacent slabs intersect the surface in this case, providing pathways along which adventitious species could easily diffuse into the film. By contrast, a film in which only the (0*k*0) facets are exposed can present a surface in which the In—I bonds are completely saturated, reducing the chance that impinging oxygen will invade the lattice either by direct reaction with the surface or through facile access to the bulk. In films fabricated on SnI_2-treated substrates, slight contributions from Sn 3d and 3d- orbitals are evident, and in those on ITO/CdS, Cd 3d/3d- peaks are also present. Cd has been previously shown to diffuse into $CH_3NH_3PbI_3$, but it is benign in small amounts.[33-34] The amount of Cd is slightly reduced when films are deposited on SnI_2-treated substrates, possibly signifying that the SnI_2 layer impedes Cd diffusion. The presence of Sn at the surface of the films, together with the observations of $InSn_2I_5$ in the XRD patterns (for high concentration SnI_2 treatment), signifies the ease with which Sn can interact with the InI film.

To evaluate the photovoltaic quality of the evaporated InI films and assess the impact of the substrate treatment, solar cells were fabricated in which these films were used as the absorber. Figure 4a shows a schematic of the solar cell architecture, using an ITO/CdS/(SnI_2)/InI/poly(3-hexylthiophene-2,5-diyl) (P3HT)/Au stack, in which CdS and P3HT are the electron and hole transport layers (ETL/HTL), respectively, and SnI_2 is used as an interface modification/growth templating layer as discussed above. Figure 4b illustrates the band positions of the ETL and HTL relative to InI, demonstrating that they are expected to be conducive to extracting and blocking the proper charge carriers. The average values of device parameters corresponding to solar cells prepared using substrates treated with 10 or 20 mg/mL SnI_2 in DMF, or untreated, are displayed in Table 2. All groups of solar cells exhibit a clear photovoltaic effect, although overall efficiency is low and significant hysteresis is evident, with forward scans yielding significantly higher efficiency than reverse. Biswas and Du[18] have calculated that V_I and V_{In} have low energy barriers for diffusion, which may contribute to the observed hysteresis. The SnI_2 treatment appears to be most beneficial at 10 mg/mL, yielding the highest J_{SC}, V_{OC}, and FF under forward scan and maintaining the highest J_{SC} under reverse scan. Under reverse scan, the efficiency monotonically decreases with strength of the SnI_2 treatment, driven predominantly by a reduction in V_{OC}. It should be noted, however, that the stabilized efficiency of several selected devices generally tends to match the forward scan efficiency better than the reverse scan efficiency. This behavior is illustrated by the *J*–*V* curves of the best-performing device plotted in Figure 4c, with the (*J*, *V*) values corresponding to the stabilized power output conditions indicated by a green star. For this device, the stabilized PCE is 0.38% (as seen in the time-resolved photocurrent plot in Figure S6), while the slow forward scan yields an efficiency of 0.44%.

Table 2. Device Parameters of InI Solar Cells[a] with Varying SnI_2 Treatment (in mg/mL), Taken from Forward (Reverse) *J*–*V* Scans.[b]

SnI_2 treatment	**V_{OC} (V)**	**J_{SC} (mA/cm²)**	**FF (%)**	**PCE (%)**
none	**0.37 ± 0.03 (0.38 ± 0.02)**	**1.90 ± 0.09 (1.66 ± 0.13)**	**38.6 ± 2.3 (34.5 ± 3.7)**	**0.28 ± 0.03 (0.22 ± 0.04)**
10	**0.45 ± 0.01 (0.33 ± 0.02)**	**2.14 ± 0.09 (1.99 ± 0.16)**	**40.2 ± 1.9 (29.7 ± 2.7)**	**0.39 ± 0.04 (0.19 ± 0.03)**

20	**0.45 ± 0.03 (0.27 ± 0.03)**	**1.84 ± 0.07 (1.83 ± 0.12)**	**38.9 ± 2.5 (30.6 ± 2.5)**	**0.32 ± 0.04 (0.15 ± 0.02)**

[a] Data are averaged over 10, 11, and 11 devices corresponding to untreated, 10 mg/mL, and 20 mg/mL SnI_2 substrate treatments, respectively.

[b] Uncertainty in the measurements is quantified by the standard deviation.

External quantum efficiency (EQE) measurement of the best-performing device (Figure 4d) yields an integrated J_{SC} of ~2.4 mA/cm^2, which is slightly higher than but reasonably close to the ~2.1 mA/cm^2 value obtained from the J–V and stabilized photocurrent measurements. This discrepancy may be at least partially attributable to the smaller illuminated (sampled) area under the EQE beam than the 0.1 cm^2 area exposed during J–V measurement, considering the possibility of spatial variations within the films composing the device. To verify that InI is the source of the photocurrent, the long-wave cutoff of the EQE spectrum is estimated by finding the maximum value of -dEQE/dλ at this point. This measurement yields a band gap of ~1.98 eV/625 nm, agreeing well with the optical and photoelectron spectroscopy measurements of the InI band gap. From the device results, the SnI_2 treatment appears to be helpful (at least to a limited extent) in boosting InI solar cell performance. The loss in performance as a result of increasing the SnI_2 concentration to 20 mg/mL is likely a consequence of electron blocking, either by the SnI_2 layer itself or the $InSn_2I_5$ product evident in the XRD patterns in Figure 3.

In summary, to more fully explore the range of lone pair metal halides and their potential use in photovoltaics, we have investigated the thin film deposition of indium(I) iodide, which has not yet been integrated into solar cells. Thin films of InI can be obtained readily by thermal evaporation, and the composition and preferred crystallographic orientation can be manipulated through the use of different substrates/additives. While the morphology of the InI films is satisfactory for device fabrication (i.e., compact and conformal grain structure), their defect properties appear to be inferior to those of halide perovskites, as exhibited by their weak photoluminescence. Furthermore, photoemission measurements indicate that the Fermi level lies at a position deep within the gap, perhaps pinned due to the Schottky defects predicted by prior calculations.[18] By modulating film growth using a SnI_2 substrate treatment, solar cells prepared using InI as the absorber generate measurable photocurrent with power conversion efficiency of up to ~0.4%, demonstrating that InI is indeed a photovoltaic material. The low performance of these solar cells may be attributable to the unfavorable defect properties of InI, suggesting that the presence of a lone-pair metal is not necessarily proof against the harmful influence of defect states near midgap (in agreement the proposition of Kurchin *et al.*[25] that lone pair metals cannot protect against deep anion vacancies). Alternatively, oxygen impurities in the lattice could also lead to deep defect states or reduce carrier mobility. The prior reports of reasonable carrier lifetime/mobility-lifetime product[13, 15, 26] suggest that it may be worthwhile to further investigate differences between InI thin films and single crystals, and develop strategies to make the former behave more like the latter.

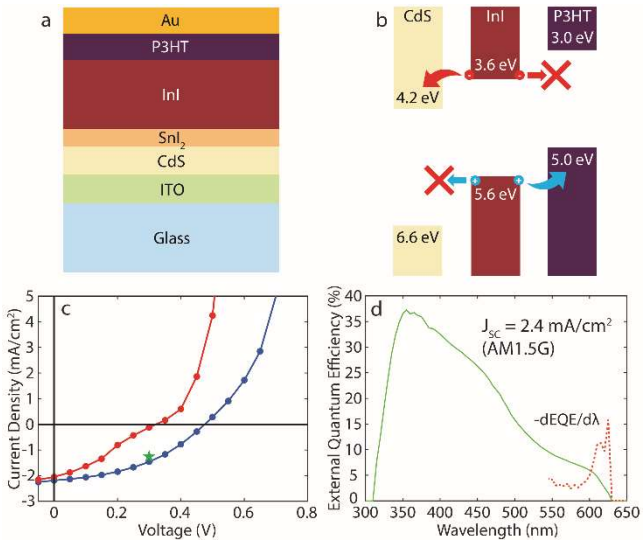

Figure 4. Device architecture (a) and band diagram (b) for the solar cells used in this work; J–V curves (c) and stabilized power parameters (indicated by green star) of the best-performing device; EQE spectrum (solid line) and its derivative (dashed line) corresponding to the same device (d).

ASSOCIATED CONTENT

Supporting Information. UV-Vis-NIR spectra of different thickness InI films, XRD pattern of SnI_2 thin film, SEM images and EDX spectra of InI films on ITO/CdS for different SnI_2 treatments, XPS spectra of InI films on different substrates, stabilized photocurrent of highest-performing solar cell, experimental methods. This material is available free of charge via the Internet at http://pubs.acs.org.

AUTHOR INFORMATION

Corresponding Author

* D. B. Mitzi. E-mail: david.mitzi@duke.edu

Author Contributions

The manuscript was written through contributions of all authors. All authors have given approval to the final version of the manuscript.

Funding Sources

The work done at Duke University and University of Toledo was funded by the Office of Energy Efficiency and Renewable Energy (EERE), U.S. Department of Energy, under Award Number DE-EE0006712 (W.A.D.-S., D.B.M., Y.Y.). W.A.D.-S. acknowledges support from the Fitzpatrick Institute for Photonics John T. Chambers Scholarship. I.G.H. acknowledges support from the NSERC Discovery Grants program (RGPIN 04809-2014) and the Canada Foundation for Innovation (CFI).

This work was performed in part at the Duke University Shared Materials Instrumentation Facility (SMIF) and at the Chapel Hill Analytical and Nanofabrication Laboratory (CHANL), members of the North Carolina Research Triangle Nanotechnology Network (RTNN), which is supported by the National Science Foundation (Grant ECCS-1542015) as part of the National Nanotechnology Coordinated Infrastructure (NNCI). All opinions expressed in this paper are the authors' and do not necessarily reflect the policies and views of DOE, NSF, NSERC, or CFI. See the Supporting Information Section of this article for more information.

Notes

The authors declare no competing financial interest.

ACKNOWLEDGMENT

The authors are grateful to Dr. A. S. Kumbhar at CHANL for assistance in collecting SEM images and EDX spectra/line scans.

ABBREVIATIONS

DMF, N,N-dimethylformamide; EDX, energy dispersive X-ray spectroscopy; EQE, external quantum efficiency; ICDD, International Centre for Diffraction Data; IPES, inverse photoemission spectroscopy; ITO, indium tin oxide; PL, photoluminescence; PMMA, poly(methyl methacrylate); P3HT, poly(3-hexylthiophene-2,5-diyl); SEM, scanning electron microscopy; UPS, ultraviolet photoelectron spectroscopy; XPS, X-ray photoelectron spectroscopy; XRD, X-ray diffraction.

REFERENCES

(1) Yin, W. J.; Shi, T.; Yan, Y. Unique Properties of Halide Perovskites as Possible Origins of the Superior Solar Cell Performance. *Adv. Mater.* **2014,** *26*, 4653-4658.

(2) Jiang, F.; Yang, D.; Jiang, Y.; Liu, T.; Zhao, X.; Ming, Y.; Luo, B.; Qin, F.; Fan, J.; Han, H.; et al. Chlorine-Incorporation-Induced Formation of the Layered Phase for Antimony-Based Lead-Free Perovskite Solar Cells. *J. Am. Chem. Soc.* **2018,** *140*, 1019-1027.

(3) Zhang, Z.; Li, X.; Xia, X.; Wang, Z.; Huang, Z.; Lei, B.; Gao, Y. High-Quality $(CH_3NH_3)_3Bi_2I_9$ Film-Based Solar Cells: Pushing Efficiency up to 1.64%. *J. Phys. Chem. Lett.* **2017,** *8*, 4300-4307.

(4) Correa-Baena, J.-P.; Nienhaus, L.; Kurchin, R. C.; Shin, S. S.; Wieghold, S.; Putri Hartono, N. T.; Layurova, M.; Klein, N. D.; Poindexter, J. R.; Polizzotti, A.; et al. A-Site Cation in Inorganic $A_3Sb_2I_9$ Perovskite Influences Structural Dimensionality, Exciton Binding Energy, and Solar Cell Performance. *Chem. Mater.* **2018,** *30*, 3734-3742.

(5) Park, B.-W.; Philippe, B.; Zhang, X.; Rensmo, H.; Boschloo, G.; Johansson, E. M. Bismuth Based Hybrid Perovskites $A_3Bi_2I_9$ (A: Methylammonium or Cesium) for Solar Cell Application. *Adv. Mater.* **2015,** *27*, 6806-6813.

(6) Greul, E.; Petrus, Michiel L.; Binek, A.; Docampo, P.; Bein, T. Highly Stable, Phase Pure $Cs_2AgBiBr_6$ Double Perovskite Thin Films for Optoelectronic Applications. *J. Mater. Chem. A* **2017,** *5*, 19972-19981.

(7) Hamdeh, U. H.; Nelson, R. D.; Ryan, B. J.; Bhattacharjee, U.; Petrich, J. W.; Panthani, M. G. Solution-Processed BiI_3 Thin Films for Photovoltaic Applications: Improved Carrier Collection via Solvent Annealing. *Chem. Mater.* **2016,** *28*, 6567-6574.

(8) Hoye, R. L. Z.; Lee, L. C.; Kurchin, R. C.; Huq, T. N.; Zhang, K. H. L.; Sponseller, M.; Nienhaus, L.; Brandt, R. E.; Jean, J.; Polizzotti, J. A.; et al. Strongly Enhanced Photovoltaic Performance and Defect Physics of Air-Stable Bismuth Oxyiodide (BiOI). *Adv. Mater.* **2017,** *29*, 1702176.

(9) Kim, Y.; Yang, Z.; Jain, A.; Voznyy, O.; Kim, G. H.; Liu, M.; Quan, L. N.; García de Arquer, F. P.; Comin, R.; Fan, J. Z.; et al. Pure Cubic-Phase Hybrid Iodobismuthates $AgBi_2I_7$ for Thin-Film Photovoltaics. *Angew. Chem. Int. Ed. Engl.* **2016,** *55*, 9586-9590.

(10) Zhu, H.; Pan, M.; Johansson, M. B.; Johansson, E. M. J. High Photon-to-Current Conversion in Solar Cells Based on Light-Absorbing Silver Bismuth Iodide. *ChemSusChem* **2017,** *10*, 2592-2596.

(11) Turkevych, I.; Kazaoui, S.; Ito, E.; Urano, T.; Yamada, K.; Tomiyasu, H.; Yamagishi, H.; Kondo, M.; Aramaki, S. Photovoltaic Rudorffites: Lead-Free Silver Bismuth Halides Alternative to Hybrid Lead Halide Perovskites. *ChemSusChem* **2017,** *10*, 3754-3759.

(12) Slavney, A. H.; Leppert, L.; Bartesaghi, D.; Gold-Parker, A.; Toney, M. F.; Savenije, T. J.; Neaton, J. B.; Karunadasa, H. I. Defect-Induced Band-Edge Reconstruction of a Bismuth-Halide Double Perovskite for Visible-Light Absorption. *J. Am. Chem. Soc.* **2017,** *139*, 5015-5018.

(13) Shah, K. S.; Bennett, P.; Moy, L. P.; Misra, M. M.; Moses, W. W. Characterization of Indium Iodide Detectors for Scintillation Studies. *Nucl. Instrum. Methods Phys. Res., Sect. A* **1996,** *380*, 215-219.

(14) Onodera, T.; Hitomi, K.; Shoji, T. Fabrication of Indium Iodide X- and Gamma-Ray Detectors. *IEEE Trans. Nucl. Sci.* **2006,** *53*, 3055-3059.

(15) Brandt, R. E.; Poindexter, J. R.; Gorai, P.; Kurchin, R. C.; Hoye, R. L. Z.; Nienhaus, L.; Wilson, M. W. B.; Polizzotti, J. A.; Sereika, R.; Žaltauskas, R.; et al. Searching for "Defect-Tolerant" Photovoltaic Materials: Combined Theoretical and Experimental Screening. *Chem. Mater.* **2017,** *29*, 4667-4674.

(16) Haxel, G. B.; Hedrick, J. B.; Orris, G. J., Rare Earth Elements - Critical Resources for High Technology. Department of the Interior, United States Geological Survey: 2015.

(17) U. S. G. S., Mineral Commodity Summaries: Indium. Department of the Interior, United States Geological Survey: 2018.

(18) Biswas, K.; Du, M.-H. First Principles Study of Native Defects in InI. *J. Appl. Phys.* **2011,** *109*, 113518.

(19) Umari, P.; Mosconi, E.; De Angelis, F. Relativistic GW Calculations on $CH_3NH_3PbI_3$ and $CH_3NH_3SnI_3$ Perovskites for Solar Cell Applications. *Sci. Rep.* **2014,** *4*, 4467.

(20) Silver, S.; Yin, J.; Li, H.; Brédas, J.-L.; Kahn, A. Characterization of the Valence and Conduction Band Levels of n = 1 2D Perovskites: A Combined Experimental and Theoretical Investigation. *Adv. Energy Mater.* **2018,** *8*, 1703468.

(21) Wang, J.; Dong, B.; Guo, H.; Yang, T.; Zhu, Z.; Hu, G.; Saito, R.; Zhang, Z. Stability and Electronic Properties of Two-Dimensional Indium Iodide. *Phys. Rev. B* **2017,** *95*, 045404.

(22) Du, M.-H.; Singh, D. J. Enhanced Born Charges in III-VII, IV-VII_2, and V-VII_3 Compounds. *Phys. Rev. B* **2010,** *82*, 045203.

(23) Du, M.-H.; Singh, D. J. Enhanced Born Charge and Proximity to Ferroelectricity in Thallium Halides. *Phys. Rev. B* **2010,** *81*, 144114.

(24) Shi, H.; Du, M.-H. Shallow Halogen Vacancies in Halide Optoelectronic Materials. *Physical Review B* **2014,** *90*, 174103.

(25) Kurchin, R. C.; Gorai, P.; Buonassisi, T.; Stevanović, V. Structural and Chemical Features Giving Rise to Defect Tolerance of Binary Semiconductors. *Chem. Mater.* **2018**, *30*, 5583-5592.

(26) Squillante, M. R.; Zhou, C.; Zhang, J.; Moy, L. P.; Shah, K. S. InI Nuclear Radiation Detectors. *IEEE Trans. Nucl. Sci.* **1993,** *40*, 364-366.

(27) Olthof, S.; Meerholz, K. Substrate Dependent Electronic Structure and Film Formation of $MAPbI_3$ Perovskites. *Sci. Rep.* **2017,** *7*, 40267.

(28) Mattox, D. M., *Handbook of Physical Vapor Deposition (PVD) Processing*. 2nd ed.; Elsevier: 2010.

(29) Wang, L.; Yang, Y.; Jin, S.; Marks, T. J. MgO(100) Template Layer for CdO Thin Film Growth: Strategies to Enhance

Microstructural Crystallinity and Charge Carrier Mobility. *Appl. Phys. Lett.* **2006,** *88*, 162115.

(30) Chen, J.; Fu, Y.; Samad, L.; Dang, L.; Zhao, Y.; Shen, S.; Guo, L.; Jin, S. Vapor-Phase Epitaxial Growth of Aligned Nanowire Networks of Cesium Lead Halide Perovskites ($CsPbX_3$, X = Cl, Br, I). *Nano Lett.* **2017,** *17*, 460-466.

(31) Lee, S. A.; Hwang, J. Y.; Kim, E. S.; Kim, S. W.; Choi, W. S. Highly Oriented $SrTiO_3$ Thin Film on Graphene Substrate. *ACS Appl. Mater. Interfaces* **2017,** *9*, 3246-3250.

(32) Bi, C.; Zheng, X.; Chen, B.; Wei, H.; Huang, J. Spontaneous Passivation of Hybrid Perovskite by Sodium Ions from Glass Substrates: Mysterious Enhancement of Device Efficiency Revealed. *ACS Energy Lett.* **2017,** *2*, 1400-1406.

(33) Dunlap-Shohl, W. A.; Younts, R.; Gautam, B.; Gundogdu, K.; Mitzi, D. B. Effects of Cd Diffusion and Doping in High-Performance Perovskite Solar Cells Using CdS as Electron Transport Layer. *J. Phys. Chem. C* **2016,** *120*, 16437-16445.

(34) Tong, G.; Song, Z.; Li, C.; Zhao, Y.; Yu, L.; Xu, J.; Jiang, Y.; Sheng, Y.; Shi, Y.; Chen, K. Cadmium-Doped Flexible Perovskite Solar Cells with a Low-Cost and Low-Temperature-Processed CdS Electron Transport Layer. *RSC Adv.* **2017,** *7*, 19457-19463.

(35) Beck, H. P. Refinement of the Structures of $InSn_2Br_5$ and $InSn_2I_5$. *Z. Anorg. Allg. Chem.* **1986,** *586*, 45-52.

(36) Becker, D.; Beck, H. P. High Pressure Study of $NH_4Pb_2Br_5$ Type Compounds. I Structural Parameters and Their Evolution under High Pressure. *Z. Anorg. Allg. Chem.* **2004,** *630*, 1924-1932.
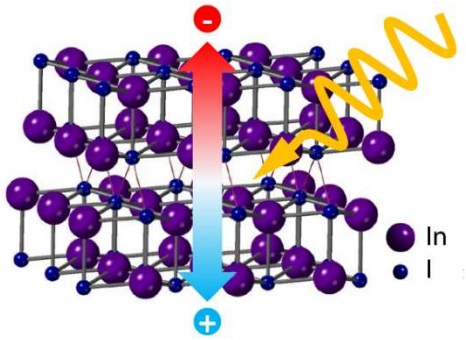
Table of Contents Figure.